Paleoceanography and Paleoclimatology

RESEARCH ARTICLE
10.1029/2020PA003900

Special Section:
The Miocene: The Future of the Past

Near-Future pCO_2 During the Hot Miocene Climatic Optimum

M. Steinthorsdottir[1,2], P. E. Jardine[3], and W. C. Rember[4]

[1]Department of Palaeobiology, Swedish Museum of Natural History, Stockholm, SE, Sweden, [2]Bolin Centre for Climate Research, Stockholm University, Stockholm, SE, Sweden, [3]Institute of Geology and Palaeontology, University of Münster, Münster, Germany, [4]Department of Geological Sciences, University of Idaho, Moscow, ID, USA

Key Points:
- Miocene Climatic Optimum proxies record high temperatures at moderate pCO_2; this cannot be replicated with existing climate models
- Either previously published records underestimate pCO_2 or climate models are missing important feedbacks
- We reconstruct moderate pCO_2 of ~450–550 ppm, implying that Earth System sensitivity must have been elevated

Supporting Information:
- Supporting Information S1
- Tables S1
- Figure S1

Correspondence to:
M. Steinthorsdottir,
margret.steinthorsdottir@nrm.se

Citation:
Steinthorsdottir, M., Jardine, P. E., & Rember, W. C. (2021). Near-future pCO_2 during the hot Miocene climatic optimum. *Paleoceanography and Paleoclimatology*, *36*, e2020PA003900. https://doi.org/10.1029/2020PA003900

Received 3 MAR 2020
Accepted 20 APR 2020
Accepted article online 12 MAY 2020

Abstract To improve future predictions of anthropogenic climate change, a better understanding of the relationship between global temperature and atmospheric concentrations of CO_2 (pCO_2), or climate sensitivity, is urgently required. Analyzing proxy data from climate change episodes in the past is necessary to achieve this goal, with certain geologic periods, such as the Miocene climatic optimum (MCO), a transient period of global warming with global temperatures up to ~7°C higher than today, increasingly viewed as good analogues to future climate under present emission scenarios. However, a problem remains that climate models cannot reproduce MCO temperatures with less than ~800 ppm pCO_2, while most previously published proxies record $pCO_2 < 450$ ppm. Here, we reconstructed MCO pCO_2 with a multitaxon fossil leaf database from the well-dated MCO Lagerstätte deposits of Clarkia, Idaho, USA, using four current methods of pCO_2 reconstructions. The methods are principally based on either stomatal densities, carbon isotopes, or a combination of both—thus offering independent results. The total of six reconstructions mostly record pCO_2 of ~450–550 ppm. Although slightly higher than previously reconstructed pCO_2, the discrepancy with the ~800 ppm required by climate models remains. We conclude that climate sensitivity was heightened during MCO, indicating that highly elevated temperatures can occur at relatively moderate pCO_2. Ever higher climate sensitivity with rising temperatures should be very seriously considered in future predictions of climate change.

1. Introduction

1.1. The Miocene Climatic Optimum

Projections of future climate predict that atmospheric CO_2 concentrations (pCO_2) will continue to increase due to human activity and reach at least 600 ppm by year 2100 under the "business as usual" scenario (IPPC report, 2014). CO_2 is a principal greenhouse gas known to cause global climate change and computer simulations based on current understanding show that these high levels will result in a global temperature increase of at least 4°C, a significant increase which will be perilous to Earth's biota and human societies (Sherwood & Huber, 2010). Yet there is still considerable uncertainty about the precise relationship between pCO_2 and the magnitude of temperature increase—i.e., Earth's climate sensitivity—and in reality the warming effect could be stronger. One of the most advantageous ways to improve our understanding of this relationship is to look to the geological record, where conditions of past climate change are documented in data archives of rocks and fossils, with past greenhouse periods in particular offering unique perspectives on the response of the Earth system to elevated pCO_2. The Miocene period (~23–5 Ma) is of particular interest when comparing to present and near future conditions, because continental positions were quite similar to today and an increasingly "modern" flora and fauna was evolving (see, e.g., Flower & Kennett, 1994 and Steinthorsdottir et al., 2020). Within this period, the early to middle Miocene Climatic Optimum (MCO, ~16.9–14.7 Ma) is the youngest of several transient warm episodes with highly elevated temperatures and perturbations of the carbon cycle, superimposed on a pattern of long-term cooling through the Cenozoic, the past 66 million years of Earth history (Holbourn et al., 2015; Pound et al., 2012; Zachos et al., 2001, 2008). It has been suggested that the MCO was caused by CO_2 outgassing from the contemporaneous volcanic emplacement that resulted in the Columbia River Basalt Group (CRBG; Barry et al., 2013; Kasbohm & Schoene, 2018). A new age model of CRBG emplacement narrows the time span of active volcanism from ~2 Ma to just 75 ka, simultaneously correlating the onset of CRBG volcanism and the onset of the MCO to less than ~100 ka, supporting the hypothesis that CRBG volcanic emissions acted as the climatic

forcing causing the MCO. A shorter duration of the CRBG emplacement would indicate a higher average pCO_2 emission volume as well as higher transient peak pCO_2 concentrations during volcanism (Kasbohm & Schoene, 2018).

A key research problem remains unsolved in relation to the MCO. Most proxy records indicate that atmospheric pCO_2 was <450 ppm during the MCO (sometimes much lower), which is close to the present and near-future pCO_2 projections. This includes pCO_2 reconstructed using the proxies paleosols (Breecker & Retallack, 2014; Ji et al., 2018; Retallack, 2009); alkenones (Zhang et al., 2013); marine boron isotopes (Badger et al., 2013; Foster et al., 2012; Greenop et al., 2014), and stomata (Grein et al., 2013; Royer, 2003; Royer et al., 2001), with only one stomatal proxy study reporting MCO pCO_2 of up to ~550 ppm (Kürschner et al., 2008). Early results based on *Metasequoia occidentalis* stomatal densities from the same Clarkia localities studied here (Royer, 2003; Royer et al., 2001) indicated low pCO_2 of ~310–315 ppm during MCO, whereas recalibration of the same data by Beerling et al. (2009) reported pCO_2 to be at least 100 ppm higher, in the 400–500 ppm range. Meanwhile, a host of terrestrial (Goldner et al., 2014; Pound et al., 2012) and marine (Lear et al., 2000; Zhang et al., 2013) paleoclimate archives demonstrate pervasive global warmth up to ~7°C above modern temperatures, unmatched since the Eocene when pCO_2 was >800 ppm. This problem is significant because no climate simulation has so far reproduced MCO warmth at less than ~800 ppm, up to twice the reconstructed pCO_2, even after imposing multiple forcings (Goldner et al., 2014). These observations imply either that important positive feedbacks are missing from the climate models (which are the same ones used for simulating future climate) or that there is a lack of knowledge of past climate forcings. Two recent studies recalibrated previously published marine carbonate and boron isotope MCO pCO_2 records, using new sensitivity analyses and laboratory experiments, and found pCO_2 levels near or exceeding 800 ppm (Sosdian et al., 2018; Stoll et al., 2019). However, these new results need to be further tested and do not explain the discrepancy with the results derived from terrestrial proxies.

Here, we present new multimethod, multitaxon pCO_2 reconstructions based on fossil leaves from sedimentary deposits in Idaho, USA, dated to have been accumulated at the height of MCO warming. Our aim was to answer the question: was pCO_2 moderately or highly elevated during the MCO?

2. Materials and Methods

2.1. The Clarkia Fossil Lagerstätte Deposits

The Clarkia fossil Lagerstätte of northern Idaho, USA, is celebrated for its extraordinary preservation of fossils, in particular the fossil flora (Rember, 1991; Smiley et al., 1975; Smiley & Rember, 1985a). The Clarkia lacustrine sedimentary deposits belong to the Latah Formation and are exposed at several localities near the small town of Clarkia, Shoshone County in Idaho (Figure 1). The sediments were deposited on the bed of a lake that formed suddenly when the Priest Rapids Member flow of the CRBG Wanapum Formation dammed the proto-St. Maries River to create the deep and elongated Miocene Clarkia Lake in the river valley (Figure 1; Smiley & Rember, 1985b; Yang et al., 1995). The lake was surrounded by dense vegetation, and the anoxic bottom conditions which developed in the lake allowed excellent preservation of the plant and animal material that was carried into the lake by wind and water, as well as of ash periodically blown in from nearby active volcanic sites (Ladderud et al., 2015; Rember, 1991; Smiley & Rember, 1985b; Wang et al., 2017). The sedimentary section consists mostly of finely laminated silt and clay and is divided into two zones: an upper oxidized zone and a lower unoxidized zone of varying thickness throughout the basin, with the best-preserved compression leaf fossils found in the lower zone, and mostly lower-quality impression leaf fossils in the upper (Smiley et al., 1975). The sediments contain numerous ash beds, some of which have been correlated to tephra deposits of known ages, enabling the dating of the duration of the Clarkia Lake and deposition of the fossil beds to ~16–15.5 Ma, attesting that the bulk of CRBG volcanism took place prior to 15.5 Ma (Ladderud et al., 2015; Nash & Perkins, 2012). Recently, the exact dating of the Clarkia Lake sediment deposition has been narrowed down to ~15.9 Ma, using sanidine K/Ar and Ar/Ar dates (Geraghty, 2017), as well as U-Pb geochronology based on zircons (Kasbohm & Schoene, 2018), from volcanic ash deposits, intercalated with the basalt stratigraphy.

The Clarkia fossil flora is very diverse and abundant, including plentiful leaves as well as reproductive organs such as flowers, seeds, nuts, fruits, and cones. The specimens are preserved essentially unaltered

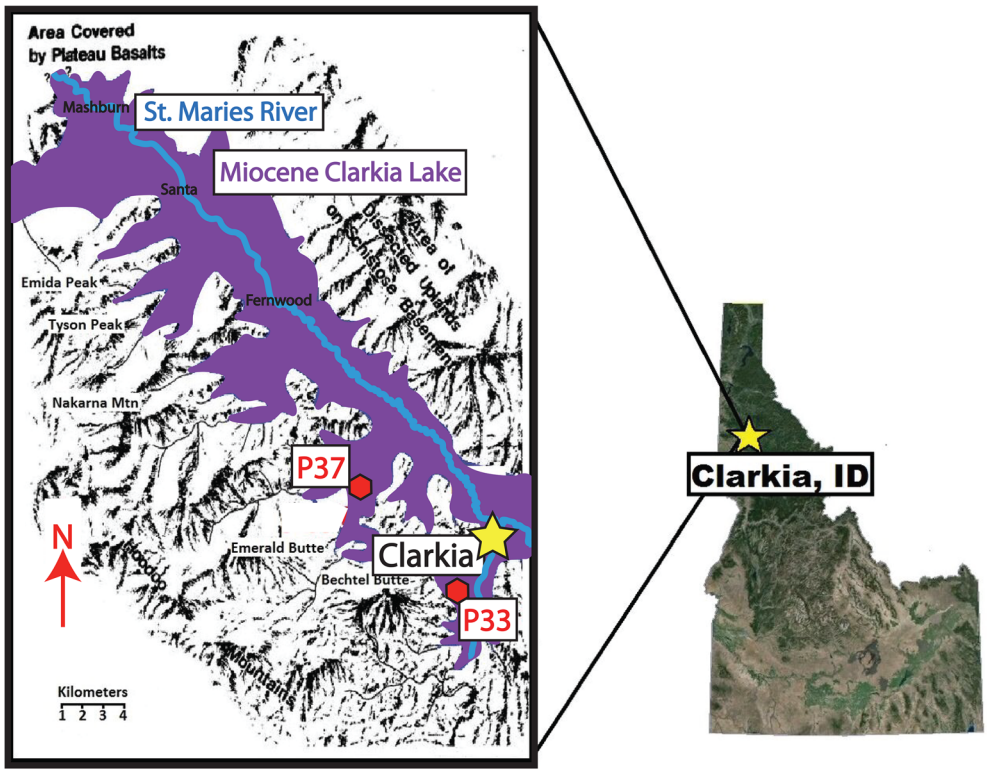

Figure 1. The Clarkia fossil lagerstätte deposits. A map of the Miocene Clarkia Lake, near the town of Clarkia, Idaho (yellow star), with the two fossil localities studied here, P-33 and P-37, marked with red hexagons. Adapted after Geraghty (2017), and Smiley et al. (1975).

since burial in the unoxidized zone—retaining epidermal and mesophyll cellular detail, sometimes with the original autumn red or summer green chlorophyll coloring showing briefly upon exposure—whereas the oxidized zone preserves (sometimes exquisite) imprints only. The flora consists of numerous angiosperms, gymnosperms, as well as some ferns and bryophytes. The closest living plant relatives now occur in the southeastern USA and southern China, and the floral composition suggests that the temperate deciduous forest grew in a warm and humid climate, very different from northern Idaho today (Denk et al., 2011; Kvaček & Rember, 2000; Pinson et al., 2018; Rember, 1991; Smiley et al., 1975; Smiley & Rember, 1981, 1985a). This is independently supported by reconstructions of annual temperature and precipitation based on local contemporaneous paleosols (Hobbs & Totman Parrish, 2016).

The leaf fossils studied here derive from two localities in the unoxidized zone, the type locality and original discovery site P-33, cropping out at the 'Fossil Bowl and racetrack' locality, as well as P-37, located on the west fork of Emerald Creek (Figure 1; Rember, 1991; Smiley et al., 1975; Smiley & Rember, 1985b). The full extent of the Clarkia sedimentary section is ~3,700 cm at the more extensive site P-33, when calculated using common ash beds at both sites, with ~3,200 cm stratigraphically logged in detail with drill cores at P-37 (Figure 2; Geraghty, 2017; Rember, 1991; Smiley & Rember, 1985b). P-37 crops out within the upper part of this range, to an approximate depth of 1,400 cm. The P-33 outcrop is ~426 cm in extent and has been correlated using tephrostratigraphy to lie ~300 cm below the bottom of the P-37 outcrop, with the top at ~1,700 cm depth in the drill core. However, the P-33 section is compressed to ~200 cm in the P-37 drill core (Geraghty, 2017). We therefore operate with two sedimentary logs for the outcrops, with the P-37 outcrop ranging 0–1,400 cm and the P-33 outcrop ranging 0–426 cm (Figure 2). Because of the different extent of the two sections, it is difficult to know the exact interval between P-37 and P-33, with the ~300 cm in the more compressed P-37 core being the minimum distance. The samples studied here derive from just above and below the pink ash bed at P-33 (Figure 2), as well as from the top ~800 m at P-37.

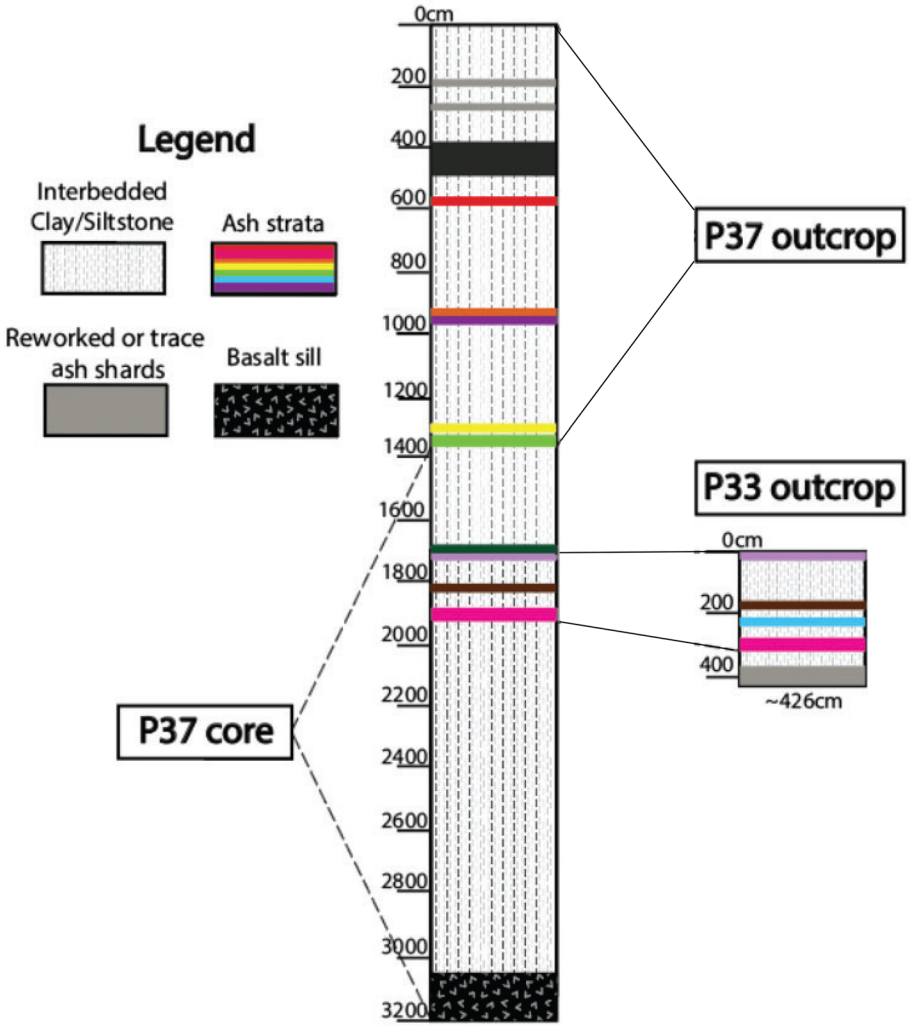

Figure 2. Stratigraphy of the Clarkia fossil lagerstätte deposits. The relative stratigraphic position of the sedimentary outcrops at localities P-33 and P-37 are indicated, as well as the P-37 core, establishing the depth of the section. Ash layers used for tephrostratigraphic correlation indicated with multicolored lines. Adapted after Geraghty (2017).

2.2. Leaf Sampling and Analysis

Blocks of sediments were dug out of the cliff faces at each locality and split open with knives to reveal fossil leaves, which were identified to lowest possible taxonomic level in the field and removed from the sediment surface (Figure 3). Each leaf was stored individually between two acetate sheets, labeled with taxon and site information and stored in refrigerators prior to analysis. In the laboratory, the leaf cuticle abaxial surfaces were photographed at 200× magnification to best capture the epidermal morphology, taking seven evenly distributed photographs away from base, apex, midrib, and margin (*sensu* Poole & Kürschner, 1999). The leaves were photographed untreated under an epifluorescent beam, using a Leica microscope with a mounted Leica camera (DF310 FX) and associated software (LAS v3.8). Images were then annotated with grids, delimiting areas of 300 × 300 μm, or 200 × 200 μm in the case of small (and thus many) cells, and all the stomata as well as the epidermal cells within each of on average five grids per leaf were counted. In addition, stomatal pore lengths and guard cell widths were measured on 10 stomata per leaf, all using the free software ImageJ (1.46 h; http://imagej.nih.gov/ij). The leaves were also sampled for $\delta^{13}C$ isotope analysis, which was performed at Iso-Analytical Limited laboratory in Crewe, Cheshire, UK. Finally, the leaves were stored individually in 5% HCl in plastic containers in the laboratory cold storage at the Swedish Museum of Natural History.

Figure 3. Fossil leaves from Clarkia. Two fossil leaves demonstrating the exquisite preservation of the Clarkia flora. (a) A Lauraceae leaf, newly excavated in the field, showing the original red autumn color, (b) *Ostrya* sp. leaf specimen between two acetate sheets, ready for analysis in the laboratory.

Following new protocols in paleo-pCO_2 reconstruction, only taxa represented by four or more specimens were included in the analyses (see, e.g., Foster et al., 2017). P-33 offered the most abundant well-preserved leaves, in a total of five taxa: *Betula vera* ($n = 8$), *B. fairii* ($n = 7$), *Ostrya* sp. ($n = 4$), *Quercus payettensis* ($n = 9$), and Lauraceae ($n = 6$). P-37 is represented by three taxa: *B. vera* ($n = 4$), *B. fairii* ($n = 4$), and *Q. payettensis* ($n = 18$). Collected leaves within the genera *Betula* and *Quercus* that could not be identified to species level were excluded from the analyses. Lauraceae leaf and cuticle morphology however are very generalized, and the leaves could not be assigned to lower taxonomic rank, which was also true for species within genus *Ostrya*. For sample images of the epidermal micromorphology of the studied leaves, detailed data on each individual leaf specimen, including stomatal density and index, measurements of pore length and guard cell width, as well as $\delta^{13}C$-isotope results, see Figure S1 and Tables S1 to S4 in the supporting information.

2.3. Paleo-pCO_2 Reconstruction

For MCO pCO_2 reconstruction based on Clarkia fossil leaves, we used three stomatal proxy methods as well as a stomata-independent carbon isotope-based method for comparison. The stomatal proxy methods are based on the inverse relationship that exists between leaf stomatal densities (SD = $N_{stomata}/mm^2$) of most woody plants and atmospheric pCO_2 (Woodward, 1987). The change in stomatal densities is the morphological expression of plants' physiological response aiming to maximize water use efficiency, that is, to minimize water loss through transpiration when CO_2 is abundantly available in the atmosphere. Stomatal plant leaf density can also be quantified as the stomatal index (SI), where both stomata and epidermal cells are counted within the annotated grids and SI calculated as SI (%) = [SD/ (SD + ED)] × 100 (where ED = $N_{epidermal\ cells}/mm^2$). SI is less affected than SD by additional environmental and physiological factors besides pCO_2, such as irradiance levels, moisture, and leaf expansion (Salisbury, 1927). The stomatal proxy methods are by now well-established in the paleoclimate literature, having been applied to a plethora of plant taxa from a wide variety of geological, ecological, and climatological backgrounds to reconstruct paleo-pCO_2 from the Paleozoic until today, generally showing remarkable intermethod consistency (e.g., Barclay & Wing, 2016; Grein et al., 2013; Kürschner et al., 2008; Li et al., 2019; Londoño et al., 2018; Mays et al., 2015; McElwain & Steinthorsdottir, 2017; Milligan et al., 2019; Montañez et al., 2016; Reichgelt et al., 2013; Royer et al., 2001; Steinthorsdottir et al., 2011, 2013; Steinthorsdottir, Porter, et al., 2016; Steinthorsdottir, Vajda, Pole, & Holdgate, 2019; Steinthorsdottir, Vajda, & Pole, 2019; Steinthorsdottir &

Vajda, 2015; Tesfamichael et al., 2017; Wagner et al., 1996; Zhou et al., 2020) and are considered one of four most useful proxies for paleo-pCO_2 (Beerling & Royer, 2011).

Three methods of stomatal proxy paleo-pCO_2 reconstruction are currently in use: (1) the empirical stomatal ratio method, which utilizes the ratio between the SD, or more usually SI, of fossil plants and the SD or SI of extant nearest living relatives or equivalents (NLR or NLE), grown in known (measured) pCO_2, to estimate paleo-pCO_2 (McElwain, 1998; McElwain & Chaloner, 1995); (2) the also empirical transfer function method, which uses herbarium and/or experimental data sets of NLR/NLE responses to variations in pCO_2 to construct regression curves on which fossil SD or SI can be plotted to infer paleo-pCO_2 (e.g., Barclay & Wing, 2016; Kürschner et al., 2008); and (3) mechanistic gas exchange modeling, which is taxon-independent and based on morphological and plant physiological measurements as well as input of additional parameters, such as leaf $\delta^{13}C$ (e.g., Franks et al., 2014; Konrad et al., 2017). Here, we used all three proxy methods—the stomatal ratio method with nine different NLE, four transfer functions, and the Franks gas-exchange model—to obtain a robust pCO_2 reconstruction for the MCO, as detailed below (see sections 2.3.1–2.3.3). To test the stomatal proxy results, we additionally applied a stomata-independent method—the C_3 proxy which utilizes fossil plant's stable carbon isotope discrimination ($\Delta^{13}C$) to reconstruct paleo-pCO_2 (Schubert & Jahren, 2012, 2015, see section 2.3.4). For all four proxy methods, confidence intervals were estimated using Monte Carlo error propagation (see section 2.3.5).

2.3.1. The Stomatal Ratio Method

In the stomatal ratio method, we employed the ratio between SI of the fossil plants and SI of the plant's NLR or NLE, in relation to the ratio between the known pCO_2 (modern, measured) and paleo-pCO_2. The ratio between SI_{modern}/SI_{fossil} and $pCO_{2\ fossil}/pCO_{2\ modern}$ is assumed to be 1:1 (McElwain, 1998), and the stomatal ratio calibration is expressed by the equation:

$$pCO_{2\ paleo} = SI_{NLE}/SI_{fossil} \times pCO_{2\ modern}. \quad (1)$$

We used several previously published SI-pCO_2 couples for each of the major groups, including *B. pendula* and *B. luminifera* (Kürschner, 1997; Sun et al., 2012; Wagner, 1998; Wagner et al., 1996) for the Betulaceae (including *B. vera*, *B. fairii*, and *Ostrya sp.*). Of these, we consider *B. luminifera* to be the best NLE for the Betulaceae studied here, based on both morphology of the leaves and their ecological preference for temperate to subtropical climate (Sun et al., 2012). *B. pendula* is morphologically a good NLE, but prefers colder climate—however, we include it here to better capture variance in SI response within the genus. *B. luminifera* SI has been reported as 10.7% at 390 ppm pCO_2 (Sun et al., 2012, their Fig. 5b) and *B. pendula* SI at 7–8.5% at 360 ppm pCO_2 (Kürschner, 1997; Wagner, 1998; Wagner et al., 1996).

For pCO_2 reconstruction based on Clarkia *Q. payettensis*, we use published SI-pCO_2 values based on the NLE species *Q. robur*, *Q. petra*, and *Q. nigra* (Beerling & Chaloner, 1993; van Hoof et al., 2006; Wagner et al., 2005). A combined *Q. robur*/*Q. petra* data set recorded SI of ~19% at 280–300 ppm (van Hoof et al., 2006), with an independent *Q. robur* study recording SI of ~21% at 345 ppm (Beerling & Chaloner, 1993). A third study recorded SI-pCO_2 couples of 22% at 320 ppm and 19.5% at 360 ppm for *Q. nigra* (Wagner et al., 2005).

For the Lauraceae data set, the four species *Litsea sebifera*, *L. fuscata*, *L. stocksii*, and *Laurus nobilis* were chosen as NLE (Kürschner et al., 2008; McElwain, 1998). The three *Litsea* subtropical–tropical south-east Asian and Indo-Malaysian rainforest tree species are the better NLE for the Miocene Lauraceae studied here and have previously been used in the stomatal ratio method reconstructing paleo-pCO_2 for the similarly warm Cenozoic interval the Eocene (McElwain, 1998; Steinthorsdottir, Vajda, & Pole, 2019), with SI_{NLE} being 19% for *L. glutinosa*, 18.3% for *L. fuscata*, and 14.4% for *L. stocksii* at 360 ppm pCO_2 (see McElwain, 1998). The evergreen Mediterranean species *L. nobilis* was originally assigned as NLE for the extinct Neogene European species *L. abchasica* for a Miocene paleo-pCO_2 reconstruction (Kürschner et al., 2008; Kürschner & Kvaček, 2009), with SI_{NLE} of 16.37–20.32% at 300 ppm. It may not be the most fitting NLE for the North American Miocene Lauraceae studied here, but we chose to include it both in the stomatal ratio and transfer function methods for easier comparison to previously published Cenozoic pCO_2 values (Kürschner et al., 2008; Steinthorsdottir, Porter, et al., 2016, Steinthorsdottir, Vajda, & Pole, 2019, Steinthorsdottir, Vajda, Pole, & Holdgate, 2019), considering it essentially as a standardized Lauraceae. SI data are provided in Table S1.

2.3.2. Transfer Functions

For the Betulaceae group, we used two transfer functions, the first one based on *B. luminifera* (Sun et al., 2012):

$$pCO_{2\ \mathrm{paleo}} = (\mathrm{SI} - 20.58)/-0.026. \quad (2)$$

For comparison, we use a second transfer function based on a mixed database of *B. pubescens* and *B. nana* (Finsinger & Wagner-Cremer, 2009):

$$pCO_{2\ \mathrm{paleo}} = 10^{(2.8687-(0.357\times\log\ (\mathrm{SIfossil})))}. \quad (3)$$

For *Q. payettensis*, we used a transfer function based on *Q. robur* (Garcia-Amorena et al., 2006).

$$pCO_{2\ \mathrm{paleo}} = -6.25 \times (\mathrm{SI}_{\mathrm{fossil}} - 71.09). \quad (4)$$

For the Lauraceae data set, we used the transfer function of Kürschner et al. (2008) constructed for Miocene extinct Lauraceae, based on the extant species *L. nobilis* calibrated from a set of historical herbarium leaves, with an added correction factor of 150 ppm, since the leaves systematically underestimated pCO_2 (see Kürschner et al., 2008 for details):

$$pCO_{2\ \mathrm{paleo}} = 10^{(3.173-(0.5499\times\log\ (\mathrm{SIfossil})))} + 150. \quad (5)$$

2.3.3. Gas-Exchange Modeling

The "Franks" gas-exchange model (Franks et al., 2014) is based on the simple and thoroughly tested Farquhar model for C3 photosynthesis, where the rate of carbon assimilation equals the product of total leaf conductance to CO_2 and the concentration gradient of atmospheric-to-leaf-internal CO_2 (Farquhar & Sharkey, 1982). The carbon isotope discrimination during photosynthesis ($\Delta^{13}C$) is also used to reconstruct the ratio of leaf-internal-to-atmospheric pCO_2 (c_i/c_a) and is determined based on measurements of plant tissue carbon isotope composition ($\delta^{13}C$) as well as an estimate of paleo-atmospheric CO_2 $\delta^{13}C$ (here −5.3 ‰ for the MCO; Tipple et al., 2010). The Franks model thus consists of two interwoven principal equations which are solved iteratively for the two unknown factors paleo-photosynthetic rate and paleo-atmospheric pCO_2:

$$C_a = pCO_{2\ \mathrm{paleo}} = A_n/\left(g_{c(op)}(1-c_i/c_a)\right), \quad (6)$$

where A_n is the net rate of CO_2 assimilation by leaves (μmol m^{-2} s^{-1}), $g_{c(op)}$ is the operational conductance to atmospheric CO_2 diffusion to photosynthesis sites within the leaf (mol m^{-2} s^{-1}), which is determined by the stomatal dimension measurements: guard cell width and stomatal pore length (GCW, PL). Key input parameters derive from stomatal morphology and carbon isotopic composition measurements on fossil leaf tissue, as well as from gas-exchange measurements on extant plants. The first of the iteratively solved equations is the Farquhar model, where total leaf conductance to pCO_2 is determined mostly by SD, GCW, and PL. The second equation, derived from an expression for Ru-BP regeneration-limited photosynthesis (Farquhar et al., 1980), describes the long-term change in photosynthetic rate due to changing atmospheric CO_2 concentration relative to known values in a nearest living relative plant. For all other input parameters for the model, we use the generic values recommended by Franks et al. (2014). This includes the angiosperm A_n (=A_0), since it is based on measurements of modern and Miocene *Betula* and *Quercus*, which is highly appropriate for our database. Input data for the Franks model are provided in Table S2.

In a second separate run of the Franks model, we use an updated s4 scaling (ratio of operating to maximum stomatal conductance) of 0.26 ± 0.11, based on a recently updated assessment of this across numerous woody angiosperm (Murray et al., 2019; see Table S3 for input data). In a third run, we used a phylogenetic correction factor for plant tissue $\delta^{13}C$ as suggested by Porter et al. (2017) which has recently been applied to the Franks model (Porter et al., 2019). This correction is intended to improve the convergence of pCO_2 estimates generated from different plant clades, and for angiosperms Porter et al. (2017) recommended a correction of −2.31‰ (see Table S4 for input data).

2.3.4. C_3 Plant Proxy Modeling

The empirical pCO_2 proxy model proposed by Schubert and Jahren (2012, 2015) is based on the relationship between pCO_2 and the stable carbon isotope discrimination ($\Delta^{13}C$) of plant tissue; $\Delta^{13}C$ is then used to back-calculate the concentration of CO_2 in the past. The model is based on the observed hyperbolic relationship between $\Delta^{13}C$ and pCO_2:

$$\Delta^{13}C = [(A)(B)(pCO_2 + C)]/[A + B \times (pCO_2 + C)]. \quad (7)$$

Where A, B, and C are curve-fitting parameters (see Schubert & Jahren, 2012 for details). The equation was constructed based on only two angiosperm species but has since been updated (Cui & Schubert, 2016; Schubert & Jahren, 2015). Because absolute $\Delta^{13}C$ values are variable among plants grown in the same conditions, the C_3 proxy is calculated using the change in $\Delta^{13}C$ relative to a reference time interval (Cui & Schubert, 2016; Schubert & Jahren, 2015). Here, we follow Schubert and Jahren (2015) and Cui and Schubert (2016) in using the Holocene average pCO_2 and $\Delta^{13}C$ as reference input conditions, using the values provided in Cui and Schubert (2016). The model has produced results that are in reasonably good agreement with other proxy methods (Cui & Schubert, 2016), but needs to be further constrained to avoid producing unrealistic (e.g., negative) pCO_2 values (Porter et al., 2019), or pCO_2 estimates with high uncertainty (Konrad et al., 2020; Lomax et al., 2019). In an independent validation of the C_3 proxy, Lomax et al. (2019) demonstrated that due to the impact of moisture availability on $\Delta^{13}C$ pCO_2 was underestimated in dryer conditions; this effect was particularly pronounced at $pCO_2 \leq 1{,}500$ ppm. The stronger control of moisture availability on $\Delta^{13}C$ relative to pCO_2 has also been noted in other studies (e.g., Kohn, 2016; Konrad et al., 2020; Schlanser et al., 2020). Since moisture availability is itself linked to factors such as precipitation, temperature, and salinity (Lomax et al., 2019), these results suggest that a range of environmental parameters could independently influence $\Delta^{13}C$ and therefore estimated pCO_2. However, since the Clarkia paleoenvironment is not thought to have been strongly water-limited we include this proxy here as a comparison with the stomata-based pCO_2 estimates. $\delta^{13}C$ data are provided in Table S1.

2.3.5. Monte Carlo Error Propagation

Here, we have followed previous studies (e.g., Cui & Schubert, 2016; Franks et al., 2014; Royer et al., 2014) in using Monte Carlo error propagation to generate confidence intervals on the $pCO2$ estimates. In this approach, rather than simply using the mean of measured parameters (e.g., SD or GCW) to calculate the variable of interest, distributions representing those parameters (usually normal distributions defined by the mean and standard deviation or standard error of the measurements and model coefficients) are repeatedly resampled and those values used in the proxy calculations (Cui & Schubert, 2016). This generates a distribution of $pCO2$ estimates that are consistent with the error distributions of the initial measurements/coefficients. From this distribution, the median can be taken as the pCO_2 estimate, and percentiles of the distribution used to define confidence intervals, typically the 16th and 84th percentiles to define a 68% confidence interval, or the 2.5th and 97.5th percentiles to define a 95% confidence interval (Cui & Schubert, 2016; Royer et al., 2014; Tables S5 and S6).

For each proxy model run, we used 10,000 sets of randomly generated input values to calculate 10,000 pCO_2 estimates. For the Franks model (Franks et al., 2014), the R code provided with the paper includes Monte Carlo error propagation and returns the resampled pCO_2 estimates as well as a summary of the distributions and other calculated parameters. Monte Carlo error propagation was also employed by Cui and Schubert (2016) for the C_3 proxy (Schubert & Jahren, 2012, 2015), and we follow the same approach here. For both the stomatal ratio and transfer function methods, we have written new resampling routines in R (R Core Team, 2018) that incorporate the error in both the fossil and NLR/NLE SI measurements. For the transfer functions we use in this study, standard errors for the regression coefficients (intercept and slope) were not provided in the original publications, and so could not be incorporated into the Monte Carlo resampling. However, in both Sun et al. (2012) and Kürschner et al. (2008), the underlying SI and pCO_2 data were provided. We therefore refit these regressions, extracted the model coefficient standard errors, and rerun the Monte Carlo error propagation to provide a comparison with the results based on just the standard error of the SI measurements. The full results of these additional analyses are provided in Table S7. We have used standard errors rather than standard deviations to define the distributions for resampling, because this better captures repeated resampling of mean stomatal parameters from a statistical population, rather than the

resampling of individual measurements that using standard deviations would simulate. After each Monte Carlo run, we first removed any invalid pCO_2 estimates (i.e., those <0 or >10^6 ppm), and then used the 16th/84th and 2.5th/97.5th percentiles to define 68% and 95% confidence intervals around the median value (the 50th percentile, which typically closely approximates the pCO_2 estimate that would be produced by the proxy without Monte Carlo resampling). We calculated the median pCO_2 plus confidence intervals for each leaf specimen (Table S5), for each taxon within each locality (Table S6), and within each locality to provide overall within-locality pCO_2 estimates. In the main paper, we report the within-taxon and within-locality pCO_2 estimates, using 95% confidence intervals because this is the usual confidence level employed to assess statistical significance and compare among estimated parameters. The specimen-level pCO_2 estimates are given in the supporting information, along with the 68% confidence intervals to provide a direct comparison with other studies (e.g., Cui & Schubert, 2016; Franks et al., 2014; Londoño et al., 2018; Porter et al., 2019; Tesfamichael et al., 2017; see Tables S5 and S6). The R code, which includes the Monte Carlo input values, is provided in the supporting information.

3. Clarkia MCO pCO_2 Reconstructions

In our quest to robustly reconstruct MCO pCO_2, we used a multitaxon database of fossil leaves collected from a well-dated sedimentary section, and preformed multiple independent pCO_2 reconstructions—using the stomatal ratio method with 10 distinct SI-NLE pairs; four transfer functions; the Franks gas exchange model, both the original version and with two separate correction factors; as well as the C_3 proxy. Using the selection of published NLE SI-pCO_2 relationships applied to our five taxa in the stomatal ratio method, this translates to a locality average pCO_2 of 476 ppm (within-taxon median range of 402–568 ppm) at P-37 and 539 ppm (within-taxon median range of 411–614 ppm) at P-33 (Table 1, Figure 4). None of the Monte Carlo pCO_2 estimates were <0 or >10^6 ppm.

The transfer function approach, using previously published transfer functions applied to our five taxa, records similar pCO_2 as the stomatal ratio method, although appreciably lower (Table 1). A median pCO_2 of 364 ppm is recorded at P-37 (within-taxon median range of 356–473 ppm) and ~468 ppm (within-taxon median range of 370–490 ppm) at P-33 (Figure 4). None of the Monte Carlo pCO_2 estimates were <0 or >10^6 ppm. Additional Monte Carlo analyses on two of the transfer functions, incorporating standard errors on the regression coefficients as well as the SI measurements, suggest that the 95% confidence intervals reported here underestimate the true confidence intervals by 30–80% (further details are provided in Table S7).

Using the Franks model for pCO_2 reconstruction (Franks et al., 2014) in its original form with our chosen input parameters (see section 2 and Table S2), the three taxa at P-37 record median pCO_2 ranging from ~456–491 ppm, with a locality median pCO_2 of 479 ppm. Median pCO_2 for the five taxa at P-33 ranges between a minimum of 364 ppm and a maximum of 609 ppm, with a locality median pCO_2 of 548 ppm (Table 1, Figure 4). None of the Monte Carlo pCO_2 estimates were <0 or >10^6 ppm. Applying the "Murray correction" (see section 2, Table S3, and Murray et al., 2019) to the Franks model, a of median pCO_2 is recorded ranging from 389 ppm to 464 ppm at P-37 and 365 ppm to 554 ppm at P-33 (Table 1, Figure 4). The locality medians recorded using the Murray correction factor are lower than for the original input ratio used in the Franks model, with pCO_2 of 405 ppm for P-37 and 480 ppm for P-33. The spread of pCO_2 estimates was larger than with the uncorrected Franks model, with 5 values >10^6 ppm and 5,103 values <0 ppm; these were removed before the median and percentiles were calculated. When applying the "Porter correction" (see section 2, Table S4, and Porter et al., 2017) to the Franks model, significantly higher pCO_2 is recorded, with a range of 675–776 ppm and a locality median of 738 ppm at P-37, and 561–988 ppm, median 882 ppm at P-33 (Table 1, Figure 4). As with the uncorrected Franks model, no invalid pCO_2 estimates were produced.

The C_3 proxy, which is independent from stomatal parameters (see methods and Schubert & Jahren, 2012, 2015), records median within-taxon pCO_2 ranging from 471 ppm to 601 ppm at P-37, with a locality median of 529 ppm (Table 1, Figure 4). At P-33, higher values of pCO_2 are recorded, between 575 and 624 ppm, with a locality median of 603 ppm. The C_3 proxy generated 8 pCO_2 estimates >10^6 ppm and

Table 1
pCO_2 Reconstruction Summary Results for Each Taxon Within Each of the Two Clarkia Localities, Derived From Monte Carlo Error Propagation

Locality	Taxon	SD (N/mm^2)	SI (%)	Stomatal ratio	Transfer function	Franks model	Franks + Murray	Franks + Porter	C_3 proxy
P-37	*B. vera*	$314^{\pm 41}$	$6.0^{\pm 0.6}$	568 (468/722)	473 (443/515)	456 (358/620)	422 (310/1080)	675 (518/984)	471 (234/1514)
	B. fairii	$401^{\pm 33}$	$8.5^{\pm 0.8}$	402 (353/493)	402 (373/445)	491 (405/715)	464 (353/1181)	776 (625/1207)	601 (290/2496)
	Q. payettensis	$816^{\pm 122}$	$14.3^{\pm 2.0}$	474 (345/582)	356 (324/372)	481 (356/730)	389 (285/846)	739 (499/1195)	526 (255/1907)
	Locality:			476 (352/651)	364 (328/498)	479 (352/717)	405 (291/950)	738 (508/1182)	529 (254/1938)
P-33	*B. vera*	$278^{\pm 66}$	$6.0^{\pm 1.0}$	559 (446/807)	470 (425/533)	609 (456/825)	554 (381/1561)	988 (682/1406)	612 (284/2826)
	B. fairii	$314^{\pm 87}$	$6.3^{\pm 1.6}$	566 (400/834)	473 (402/538)	564 (422/1007)	528 (366/1594)	920 (650/1662)	624 (293/2768)
	Ostrya sp.	$311^{\pm 55}$	$6.0^{\pm 1.0}$	614 (446/755)	488 (425/523)	537 (415/793)	498 (359/1356)	830 (642/1320)	577 (282/2231)
	Q. payettensis	$760^{\pm 111}$	$12.0^{\pm 2.4}$	560 (419/751)	370 (345/389)	535 (400/748)	430 (321/929)	870 (607/1241)	609 (288/2569)
	Lauraceae	$723^{\pm 228}$	$14.5^{\pm 2.1}$	411 (352/570)	490 (465/556)	364 (301/618)	365 (277/831)	561 (433/1170)	575 (259/2768)
	Locality:			539 (361/797)	468 (348/543)	548 (323/848)	480 (306/1298)	882 (477/1413)	603 (281/2675)

Note. SD = stomatal density and SI = stomatal index. For each of the six proxies, the pCO_2 estimate is provided as well as the lower and upper bounds of a 95% confidence interval.

2,811 estimates <0 ppm, which were removed prior to calculating the median and percentiles of the distribution.

Summarizing the results, an obvious pattern is that the majority of the pCO_2 reconstructions are considerably lower than the ~800 ppm believed to be necessary to reproduce MCO temperatures (Figure 4, Goldner et al., 2014), even taken the errors into account, which are quite extensive for many of the proxies. Most median pCO_2 estimates converge around close to 450–550 ppm. Another clear feature is that median pCO_2 is consistently higher at P-33, the older locality, than it is at the younger locality P-37.

4. Discussion

The SI and gas exchange based methods (with the exception of Franks + Porter) recorded remarkably similar pCO_2, as has previously been shown to be the case in numerous studies (see, e.g., McElwain & Steinthorsdottir, 2017; Montañez et al., 2016; Steinthorsdottir, Vajda, & Pole, 2019; Zhou et al., 2020). The transfer function approach on the other hand recorded consistently lower pCO_2 than the other proxies, a phenomenon that has also been previously observed (Kürschner et al., 2008; Steinthorsdottir, Porter, et al., 2016, Steinthorsdottir, Vajda, & Pole, 2019, Steinthorsdottir, Vajda, Pole, & Holdgate, 2019). The stomata-independent C3 proxy recorded higher pCO_2 on average than the stomata-dependent methods, but still sufficiently similar to be regarded as independently supporting the stomata proxy results (Figure 4).

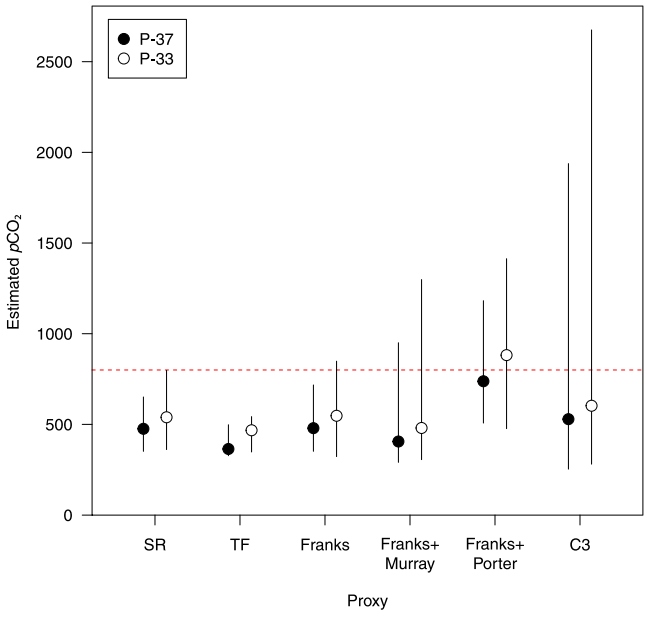

Figure 4. Clarkia MCO pCO_2 reconstruction results plotted for each proxy method at both localities, P-37 and P-33. SR = stomatal ratio, TF = transfer functions. Error bars show the 95% confidence interval. Red dashed line at 800 ppm illustrates the pCO_2 necessary to reproduce MCO temperatures in climate models (Goldner et al., 2014). Most reconstructed median pCO_2 plot in the 450–550 ppm interval.

The 95% confidence intervals on our pCO_2 estimates are derived from Monte Carlo error propagation. As such, they represent an honest accounting of the errors on the measurements and model parameters that underpin the different proxies and allow us to assess robustly how consistent our data are with different pCO_2 scenarios. The stomatal ratio, transfer function, and Franks model pCO_2 estimates all have confidence intervals that either do not overlap, or overlap only slightly, with the 800 ppm pCO_2 that is required by climate simulations to produce MCO temperatures (Goldner et al., 2014). Therefore, even with full error propagation, the results from these proxies are not consistent with such highly elevated pCO_2 levels. The Murray correction to the Franks model results in a skewed distribution with a long tail of high of pCO_2 estimates that extend well beyond 800 ppm (Figure 4), despite having a lower median than the uncorrected Franks model. The right

skewed distribution is likely to be in part a result of the removal of the high number of negative pCO_2 estimates prior to calculating the distribution percentiles: Of 61,000 resamples (61 samples × 10,000 Monte Carlo resamples), 5,103 or 8.4% were negative. Our results therefore suggest that applying the Murray correction to the Franks model amplifies the variability in the underlying measurements to the point where a high proportion of invalid pCO_2 values are produced and the final pCO_2 estimate has a low precision. The C_3 proxy resulted in 2,811 or 4.6% negative resamples and has an even more pronounced right skewed distribution that incorporates a range of unrealistic pCO_2 estimates for the MCO (i.e., up to ~2,600 ppm for site P-33, see Figure 4). Such wide confidence intervals appear to be a general issue with the C_3 proxy, when calculated relative to the Holocene reference and with Monte Carlo error propagation (Lomax et al., 2019). We therefore consider these high values to be properties of the underlying proxies, rather than reasonable pCO_2 expectations for the MCO, and suggest that further corrections may be required to increase the precision of these models.

The one exception to our pCO_2 proxy reconstructions is the Franks model with the Porter correction, which places pCO_2 at ~800 ppm. While this is consistent with the modeled pCO_2 necessary to simulate MCO temperatures (Goldner et al., 2014), we consider these estimates to be erroneously high given the results from the other proxies, including those that are based solely on SI and therefore cannot be biased by $\delta^{13}C$ measurements. This suggests that the correction to $\delta^{13}C$ suggested by Porter et al. (2017) to account for phylogenetic offsets among major plants clades leads to overestimated pCO_2 when applied to angiosperms. As noted by Porter et al. (2017), Porter et al. (2019), this is a post-hoc correction that has been developed from plants grown in experimentally controlled, growth-room conditions, and it may be that these do not successfully translate across to plants that existed in natural habitats (Lomax et al., 2019). Our results also illustrate the general point that a correction to make pCO_2 estimates from different plant groups converge better does not necessarily mean that they will converge at the right level. However, we fully acknowledge that our results only pertain to one plant clade (angiosperms) from one time and place and that this does not rule out the need for such correction factors or contradict the values put forward by Porter et al. (2017) for gymnosperms or spore producing plants. For future studies, it will be useful to investigate several different plant clades, including both spore and seed producing plants, from the same deposits, and compare pCO_2 estimates from multiple proxies (including those that do not rely on $\delta^{13}C$). This will allow phylogenetic $\delta^{13}C$ offsets to be assessed in "natural" conditions and will enable a better understanding of how these offsets impact on multitaxon pCO_2 reconstructions, both from taxa cooccurring in the same deposits and when individual measurements are compiled into long timeseries (e.g., Porteret al., 2019).

An interesting feature of the dataset is the consistent difference in pCO_2 recorded between the two localities, with higher pCO_2 recorded by all taxa and all proxies at the older P-33 compared to the younger P-37. Although this cannot be shown in a robust statistical sense and might be the result of random sampling variation, it is noteworthy that the offset is consistent across the different proxies (whether they use SI, $\delta^{13}C$, or both). The Clarkia Lake was formed when a CRBG flow, in connection with a volcanic eruption and thus CO_2 outgassing, dammed a valley river (Kasbohm & Schoene, 2018; Smiley & Rember, 1985b; Yang et al., 1995), and it is possible, perhaps even likely, that pCO_2 was indeed higher closer in time to this damming event, when P-33 sediments were being deposited. It would be highly beneficial to our understanding of Earth system processes to be able to record in detail the behavior of the carbon cycle during volcanic emplacement, and further studies are under way at the Clarkia localities to construct more high-chronological resolution fossil leaf databases to test this.

Comparing the results presented here with previously published MCO pCO_2 records, most of which record pCO_2 around or even considerably lower than ~400–450 ppm during the MCO (Badger et al., 2013; Beerling et al., 2009; Breecker & Retallack, 2014; Foster et al., 2012; Greenop et al., 2014; Grein et al., 2013; Ji et al., 2018; Retallack, 2009; Royer, 2003; Royer et al., 2001; Zhang et al., 2013), the new multimethod, multitaxon Clarkia pCO_2 record slightly corrects these estimates upwards, supporting the results of Kürschner et al. (2008), who reported MCO pCO_2 of up to ~550 ppm. Considering the confidence intervals, MCO pCO_2 presented here may also have been lower (down to ~350 ppm), but given the mutually supporting convergence of most of the proxies around median values of ~450–550 ppm, as well as the consistently high temperatures recorded by numerous proxies, we consider this higher interval to be a more likely scenario.

5. Conclusions

The multimethod, multitaxon pCO_2 reconstruction presented here indicates that pCO_2 was moderately elevated at ~450–550 ppm during the MCO. These results are somewhat higher than most previously published pCO_2 records, which generally report $pCO_2 < 450$ ppm (see Foster et al., 2017), but still considerably lower pCO_2 than climate modeling requires to reproduce MCO temperatures (Goldner et al., 2014). This indicates that climate sensitivity must have been elevated during the MCO, leading to highly elevated temperatures at moderately elevated pCO_2. With 415 ppm measured for the first time in spring 2019 (NOAA data at esrl.noaa.gov), and with no sign yet of decreasing emissions, we are fast approaching MCO-level pCO_2. The race is now on to improve our knowledge of the Earth system in order to understand whether such moderate levels of pCO_2 may also cause a devastating temperature increase of up to 7°C in the (near?) future, and if so, take action to prevent it.

Conflict of Interest

The authors declare no conflict of interest.

Acknowledgments

We thank H. K. Coxall and P. Pearson for assistance in the field and C. Geraghty, W.M. Kürschner, C.A. E. Strömberg, B. Lomax, and M. Huber for helpful discussions. Special thanks to M. J. Kohn for suggesting studying the Clarkia fossils to M. S. The fossil leaf database is stored at the Department of Palaeobiology, Swedish Museum of Natural History. All data and proxy model inputs are available in the supporting information and in the Bolin Centre for Climate Research (Stockholm University) database: https://doi.org/10.17043/steinthorsdottir-2020

References

Badger, M. P. S., Lear, C. H., Pancost, R. D., Foster, G. L., Bailey, T. R., Leng, M. J., & Abels, H. A. (2020). CO_2 drawdown following the middle Miocene expansion of the Antarctic Ice Sheet. *Paleoceanography and Paleoclimatology*, *28*(1), 42–53. https://doi.org/10.1002/palo.20015

Barclay, R. S., & Wing, S. L. (2016). Improving the Ginkgo CO_2 barometer: Implications for the early Cenozoic atmosphere. *Earth and Planetary Science Letters*, *439*, 158–171. https://doi.org/10.1016/j.epsl.2016.01.012

Barry, T. L., Kelley, S. P., Reidel, S. P., Camp, V. E., Self, S., Jarboe, N. A., et al. (2013). Eruption chronology of the Columbia River Basalt Group. *Geological Society of America Special Papers*, *497*, 45–66.

Beerling, D. J., & Chaloner, W. G. (1993). Evolutionary responses of stomatal density to global CO_2 change. *Biological Journal of the Linnean Society*, *48*(4), 343–353. https://doi.org/10.1111/j.1095-8312.1993.tb02096.x

Beerling, D. J., Fox, A., & Anderson, C. W. (2009). Quantitative uncertainty analyses of ancient atmospheric CO_2 estimates from fossil leaves. *American Journal of Science*, *309*(9), 775–787. https://doi.org/10.2475/09.2009.01

Beerling, D. J., & Royer, D. L. (2011). Convergent Cenozoic CO_2 history. *Nature Geoscience*, *4*(7), 418–420. https://doi.org/10.1038/ngeo1186

Breecker, D. O., & Retallack, G. J. (2014). Refining the pedogenic carbonate atmospheric CO_2 proxy and application to Miocene CO_2. *Palaeogeography, Palaeoclimatology, Palaeoecology*, *406*, 1–8. https://doi.org/10.1016/j.palaeo.2014.04.012

Cui, Y., & Schubert, B. A. (2016). Quantifying uncertainty of past pCO2 determined from changes in C3 plant carbon isotope fractionation. *Geochimica et Cosmochimica Acta*, *172*, 127–138. https://doi.org/10.1016/j.gca.2015.09.032

Denk, T., Grímsson, F., Zetter, R., & Símonarson, L. A. (2011). Chapter 4. The Archaic Floras. In T. Denk, F. Grímsson, R. Zetter, & L. A. Símonarson (Eds.), *Late Cainozoic Floras of Iceland. 15 Million Years of Vegetation and Climate History in the Northern North Atlantic. Topics in Geobiology, 35*, (pp. 173–231). Dordrecht: Springer.

Farquhar, G. D., & Sharkey, T. D. (1982). Stomatal conductance and photosynthesis. *American Review of Plant Physiology*, *33*(1), 317–345. https://doi.org/10.1146/annurev.pp.33.060182.001533

Farquhar, G. D., von Caemmerer, S. V., & Berry, J. A. (1980). A biochemical model of photosynthetic CO_2 assimilation in leaves of C3 species. *Planta*, *149*(1), 78–90. https://doi.org/10.1007/BF00386231

Finsinger, W., & Wagner-Cremer, F. (2009). Stomatal-based inference models for reconstruction of atmospheric CO_2 concentration: A method assessment using a calibration and validation approach. *The Holocene*, *19*, 757–764.

Flower, B. P., & Kennett, J. P. (1994). The middle Miocene climatic transition: East Antarctic ice sheet development, deep ocean circulation and global carbon cycling. *Palaeogeography, Palaeoclimatology, Palaeoecology*, *108*(3-4), 537–555. https://doi.org/10.1016/0031-0182(94)90251-8

Foster, G. L., Lear, C. H., & Rae, J. W. B. (2012). The evolution of pCO_2, ice volume and climate during the Middle Miocene. *Earth and Planetary Science Letters*, *341-344*, 243–254, DOI: https://doi.org/10.1016/j.epsl.2012.06.007

Foster, G. L., Royer, D. L., & Lunt, D. J. (2017). Future climate forcing potentially without precedent in the last 420 million years. *Nature Communications*, *8*(1), 14,845. https://doi.org/10.1038/ncomms14845

Franks, P. J., Royer, D. L., Beerling, D. J., Van de Water, P. K., Cantrill, D. J., Barbour, M. M., & Berry, J. A. (2014). New constraints on atmospheric CO_2 concentration for the Phanerozoic. *Geophysical Research Letters*, *41*, 4685–4694.

Garcia-Amorena, I., Wagner, F., van Hoof, T. B., & Gómez Manzaneque, F. (2006). Stomatal responses in deciduous oaks from southern Europe to the anthropogenic atmospheric CO_2; refining the stomatal-based CO_2 proxy. *Review of Palaeobotany and Palynology*, *141*(3-4), 303–312. https://doi.org/10.1016/j.revpalbo.2006.06.002

Geraghty, C. S. (2017). *Tephrochronology of the mid-Miocene Clarkia Lake Sedimentary Deposits*, (p. 97). M.Sc. thesis: Washington State University.

Goldner, A., Herold, N., & Huber, M. (2014). The challenge of simulating the warmth of the mid-Miocene climatic optimum. *Climate of the Past*, *10*(2), 523–536. https://doi.org/10.5194/cp-10-523-2014

Greenop, R., Foster, G. L., Wilson, P. A., & Lear, C. H. (2014). Middle-Miocene climate instability associated with high-amplitude CO_2 variability. *Paleoceanography*, *29*(9), 845–853. https://doi.org/10.1002/2014PA002653

Grein, M., Oehm, C., Konrad, W., Utescher, T., Kunzmann, L., & Roth-Nebelsick, A. (2013). Atmospheric CO_2 from the Late Oligocene to early Miocene based on photosynthesis data and fossil leaf characteristics. *Palaeogeography, Palaeoclimatology, Palaeoecology*, *374*, 41–51. https://doi.org/10.1016/j.palaeo.2012.12.025

Hobbs, K. M., & Totman Parrish, J. (2016). Miocene global change recorded in Columbia River basalt-hosted paleosols. *GSA Bulletin*, *128*(9-10), 1543–1554. https://doi.org/10.1130/B31437.1

Holbourn, A. E., Kuhnt, W., Kochhann, K. G. D., Andersen, N., & Meier, K. J. S. (2015). Global perturbation of the carbon cycle at the onset of the Miocene climatic optimum. *Geology*, *43*(2), 123–126. https://doi.org/10.1130/G36317.1

IPCC (2014). Climate Change 2014: Synthesis Report. *Contribution of Working Groups I, II and III to the Fifth Assessment Report of the Intergovernmental Panel on Climate Change* [Core Writing Team, R.K. Pachauri and L.A. Meyer (eds.)]. IPCC, Geneva, Switzerland, 151 pp.

Ji, S., Nie, J., Lechler, A., Huntington, K. W., Heitmann, E. O., & Breecker, D. O. (2018). A symmetrical CO_2 peak and asymmetrical climate change during the middle Miocene. *Earth and Planetary Science Letters*, *499*, 134–144. https://doi.org/10.1016/j.epsl.2018.07.011

Kasbohm, J., & Schoene, B. (2018). Rapid eruption of the Columbia River flood basalt and correlation with the mid-Miocene climate optimum. *Science Advances*, *4*, 1–8.

Kohn, M. J. (2016). Carbon isotope discrimination in C3 land plants is independent of natural variations in pCO_2. *Geochemical Perspectives Letters*, *2*, 35–43.

Konrad, W., Katul, G., Roth-Nebelsick, A., & Grein, M. (2017). A reduced order model to analytically infer atmospheric CO_2 concentration from stomatal and climate data. *Advances in Water Resources*, *104*, 145–157. https://doi.org/10.1016/j.advwatres.2017.03.018

Konrad, W., Royer, D. L., Franks, P. J., & Roth-Nebelsick, A. (2020). Quantitative critique of leaf-based paleo-CO_2 proxies: Consequences for their reliability and applicability. *Geological Journal*, *1*, 17. https://doi.org/10.1002/gj.3807

Kürschner, W. M. (1997). The anatomical diversity of recent and fossil leaves of the durmast oak (*Quercus petraea* Lieblein/*Q. pseudo-castanea* Goeppert)—Implications for their use as biosensors of palaeoatmospheric CO_2 levels. *Review of Palaeobotany and Palynology*, *96*(1-2), 1–30. https://doi.org/10.1016/S0034-6667(96)00051-6

Kürschner, W. M., & Kvaček, Z. (2009). Oligocene–Miocene CO_2 fluctuations, climatic and palaeofloristic trends inferred from fossil plant assemblages in Central Europe. *Bulletin of Geosciences*, *84*, 189–202.

Kürschner, W. M., Kvaček, Z., & Dilcher, D. L. (2008). The impact of Miocene atmospheric carbon dioxide fluctuations on climate and the evolution of terrestrial ecosystems. *Proceedings of the National Academy of the Sciences of the United States of America*, *105*, 449–453.

Kvaček, Z., & Rember, W. C. (2000). Shared Miocene conifers of the Clarkia flora and Europe. *Acta Universitatis Carolinae Geologica*, *44*, 75–85.

Ladderud, J. A., Wolff, J. A., Rember, W. C., & Brueseke, M. E. (2015). Volcanic ash layers in the Miocene Lake Clarkia beds: Geochemistry, regional correlation, and the age of the Clarkia flora. *Northwest Science*, *89*(4), 309–323. https://doi.org/10.3955/046.089.0402

Lear, C. H., Elderfield, H., & Wilson, P. A. (2000). Cenozoic deep-sea temperatures and global ice volumes from Mg/Ca in benthic foraminiferal calcite. *Science*, *287*(5451), 269–272. https://doi.org/10.1126/science.287.5451.269

Li, H., Yu, J., McElwain, J. C., Yiotis, C., & Chen, Z.-Q. (2019). Reconstruction of atmospheric CO_2 concentration during the late Changhsingian based on fossil conifers from the Dalong Formation in South China. *Palaeogeography, Palaeoclimatology, Palaeoecology*, *519*, 37–48. https://doi.org/10.1016/j.palaeo.2018.09.006

Lomax, B. H., Lake, J. A., Leng, M. J., & Jardine, P. E. (2019). An experimental evaluation of the use of Δ13C as a proxy for palaeoatmospheric CO2. *Geochimica et Cosmochimica Acta*, *247*, 162–174. https://doi.org/10.1016/j.gca.2018.12.026

Londoño, L., Royer, D. L., Jaramillo, C., Escobar, J., Foster, D. A., Cárdenas-Rozo, A. L., & Wood, A. (2018). Early Miocene CO_2 estimates from a Neotropical fossil leaf assemblage exceed 400 ppm. *American Journal of Botany*, *105*(11), 1929–1937. https://doi.org/10.1002/ajb2.1187

Mays, C., Steinthorsdottir, M., & Stillwell, J. D. (2015). Climatic implications of *Ginkgoites waarensis* Douglas emend. From the south polar Tupuangi flora, late cretaceous (Cenomanian), Chatham Islands. *Palaeogeography, Palaeoclimatology, Palaeoecology*, *438*, 308–326. https://doi.org/10.1016/j.palaeo.2015.08.011

McElwain, J. C. (1998). Do fossil plants signal palaeoatmospheric carbon dioxide concentration in the geological past? *Philosophical Transactions of the Royal Society of London B*, *353*(1365), 83–96. https://doi.org/10.1098/rstb.1998.0193

McElwain, J. C., & Chaloner, W. G. (1995). Stomatal density and index of fossil plants track atmospheric carbon-dioxide in the Paleozoic. *Annals of Botany*, *76*(4), 389–395. https://doi.org/10.1006/anbo.1995.1112

McElwain, J. C., & Steinthorsdottir, M. (2017). Palaeoecology, ploidy, palaeoatmospheric composition and developmental biology: A review of the multiple uses of fossil stomata. *Plant Physiology*, *174*(2), 650–664. https://doi.org/10.1104/pp.17.00204

Milligan, J. N., Royer, D. L., Franks, P. J., Upchurch, G. R., & McKee, M. L. (2019). No evidence for a large atmospheric CO_2 spike across the Cretaceous-Paleogene boundary. *Geophysical Research Letters*, *46*, 3462–3472. https://doi.org/10.1029/2018GL081215

Montañez, I. P., McElwain, J. C., Poulsen, C. J., White, J. D., DiMichele, W. A., Wilson, J. P., et al. (2016). Climate, pCO_2 and terrestrial carbon cycle linkages during late Palaeozoic glacial-interglacial cycles. *Nature Geoscience*, *9*(11), 824–828. https://doi.org/10.1038/ngeo2822

Murray, M., Soh, W. K., Yiotis, C., Spicer, R. A., Lawson, T., & McElwain, J. C. (2019). Consistent relationship between field-measured stomatal conductance and theoretical maximum stomatal conductance in C3 woody angiosperms in four major biomes. *International Journal of Plant Sciences*, *181*(1), 142–154. https://doi.org/10.1086/706260

Nash, B. P., & Perkins, M. E. (2012). Neogene fallout tuffs from the Yellowstone hotspot in the Columbia plateau region, Oregon, Washington and Idaho, USA. *PLOS ONE*, *7*(10), e44205. https://doi.org/10.1371/journal.pone.0044205

Pinson, J. B., Manchester, S. R., & Sessa, E. B. (2018). *Culcita remberi* sp. nov., an understory fern of Cyatheales from the Miocene of northern Idaho. *International Journal of Plant Science*, *179*(8), 635–639. https://doi.org/10.1086/698938

Poole, I., & Kürschner, W. M. (1999). Stomatal density and index: The practice. In T. P. Jones, & N. P. Rowe (Eds.), *Fossil Plants and Spores: Modern Techniques*, (pp. 257–260). London: The Geological Society.

Porter, A. S., & Evans-Fitz.Gerald, C., Yiotis, C., Montañez, I. P., & McElwain, J. C. (2019). Testing the accuracy of new palaeoatmospheric CO_2 proxies based on plant stable carbon isotopic composition and stomatal traits in a range of simulated palaeoatmospheric O_2:CO_2 ratios. *Geochimica et Cosmochimica Acta*, *259*, 69–90. https://doi.org/10.1016/j.gca.2019.05.037

Porter, A. S., Yiotis, C., Montañez, I. P., & McElwain, J. C. (2017). Evolutionary differences in $\Delta^{13}C$ detected between spore and seed bearing plants following exposure to a range of atmospheric O_2:CO_2 ratios; implications for palaeoatmosphere reconstruction. *Geochimica et Cosmochimica Acta*, *213*, 517–533. https://doi.org/10.1016/j.gca.2017.07.007

Pound, M., Haywood, A. M., Salzman, U., & Riding J. B. (2012). Global vegetation dynamics and latitudinal temperature gradients during the Mid to Late Miocene (15.97–5.33 Ma). *Earth-Science Review*, *112*(1-2), 1–22, https://doi.org/10.1016/j.earscirev.2012.02.005

R Core Team (2018). *R: A Language and Environment for Statistical Computing. R Foundation for Statistical Computing*, Vienna: https://www.R-project.org

Reichgelt, T., Kennedy, E. M., Mildenhall, D. C., Conran, J. G., Greenwood, D. R., & Lee, D. E. (2013). Quantitative palaeoclimate estimates for Early Miocene southern New Zealand: Evidence from Foulden maar. *Palaeogeography, Palaeoclimatology, Palaeoecology*, *378*, 36–44. https://doi.org/10.1016/j.palaeo.2013.03.019

Rember, W. C. (1991). *Stratigraphy and Paleobotany of Miocene Lake Sediments near Clarkia, Idaho*. Moscow. Ph.D. Dissertation: Univ. of Idaho.

Retallack, G. J. (2009). Greenhouse crises of the past 300 million years. *Geological Society of America Bulletin*, *121*(9-10), 1441–1455. https://doi.org/10.1130/B26341.1

Royer, D. L. (2003). Estimating latest cretaceous and tertiary atmospheric CO_2 from stomatal indices. In S. L. Wing, P. D. Gingerich, B. Schmitz, & E. Thomas (Eds.), *Causes and consequences of globally warm climates in the early Paleogene*, *Geological Society of America Special Paper*, (Vol. 369, pp. 79–93). Geological Society of America. https://doi.org/10.1130/SPE369

Royer, D. L., Donnadieu, Y., Park, J., Kowalczyk, J., & Godderis, Y. (2014). Error analysis of CO_2 and O_2 estimates from the long-term geochemical model GEOCARBSULF. *American Journal of Science*, *314*, 1259–1283. https://doi.org/10.2475/09.2014.01

Royer, D. L., Wing, S. L., Beerling, D. J., Jolley, D. W., Koch, P. L., Hickey, L. J., & Berner, R. A. (2001). Paleobotanical evidence for near present-day levels of atmospheric CO_2 during part of the tertiary. *Science*, *292*(5525), 2310–2313. https://doi.org/10.1126/science.292.5525.2310

Salisbury, E. J. (1927). On the causes and ecological significance of stomatal frequency, with special reference to the woodland flora. *Philosophical Transactions of the Royal Society of London B*, *216*, 1–65.

Schlanser, K., Diefendorf, A. F., Greenwood, D. R., Mueller, K. E., West, C. K., Lowe, A. J., et al. (2020). On geologic timescales, plant carbon isotope fractionation responds to precipitation similarly to modern plants and has a small negative correlation with pCO_2. *Geochimica et Cosmochimica Acta*, *270*, 264–281. https://doi.org/10.1016/j.gca.2019.11.023

Schubert, B. A., & Jahren, A. H. (2012). The effect of atmospheric CO_2 concentration on carbon isotope fractionation in C3 land plants. *Geochimica et Cosmochimica Acta*, *96*, 29–43. https://doi.org/10.1016/j.gca.2012.08.003

Schubert, B. A., & Jahren, A. H. (2015). Global increase in plant carbon isotope fractionation following the last glacial maximum caused by increase in atmospheric pCO_2. *Geology*, *43*(5), 435–438. https://doi.org/10.1130/G36467.1

Sherwood, S. C., & Huber, M. (2010). An adaptability limit to climate change due to heat stress. *Proceedings of the National Academy of Sciences of the United States of America*, *107*, 9552–9555.

Smiley, C. J., Gray, J., & Huggins, M. (1975). Preservation of Miocene fossils in unoxidized lake deposits, Clarkia, Idaho. *Journal of Paleontology*, *49*, 833–844.

Smiley, C. J., & Rember, W. C. (1981). Paleoecology of the Miocene Clarkia Lake (northern Idaho) and its environs. In J. Gray, A. J. Boucot, & W. B. N. Berry (Eds.), *Communities of the Past*, (551–590). Stroudsburg: PA, Hutchinson & Ross.

Smiley, C. J., & Rember, W. C. (1985a). Composition of the Miocene Clarkia flora. In C. J. Smiley (Ed.), *Late Cenozoic History of the Pacific Northwest*, (pp. 95–112). San Francisco: Pacific Division of the American Association for the Advancement of Science.

Smiley, C. J., & Rember, W. C. (1985b). Physical settings of the Miocene Clarkia fossil beds. In C. J. Smiley (Ed.), *Late Cenozoic History of the Pacific Northwest*, (pp. 11–31). San Francisco: Pacific Division of the American Association for the Advancement of Science.

Sosdian, S. M., Greenop, R., Hain, M. P., Foster, G. L., Pearson, P. N., & Lear, C. H. (2018). Constraining the evolution of Neogene Ocean carbonate chemistry using the boron isotope pH proxy. *Earth and Planetary Science Letters*, *498*, 362–376. https://doi.org/10.1016/j.epsl.2018.06.017

Steinthorsdottir, M., Coxall, H. K., de Boer, A. M., Huber, M., Barbolini, N., Bradshaw, C., et al. (2020). The Miocene: the Future of the Past. *Paleoceanography and Paleoclimatology*, *35*, e2020PA004037. https://doi.org/10.1029/2020PA004037

Steinthorsdottir, M., Jeram, A. J., & McElwain, J. C. (2011). Extremely elevated CO_2 concentrations at the Triassic/Jurassic boundary. *Palaeogeography, Palaeoclimatology, Palaeoecology*, *308*(3-4), 418–432. https://doi.org/10.1016/j.palaeo.2011.05.050

Steinthorsdottir, M., Porter, A., Holohan, A., Kunzmann, L., Collinson, M., & McElwain, J. C. (2016). Fossil plant stomata indicate decreasing atmospheric CO_2 prior to the Eocene-Oligocene boundary. *Climate of the Past*, *12*(2), 439–454. https://doi.org/10.5194/cp-12-439-2016

Steinthorsdottir, M., & Vajda, V. (2015). Early Jurassic (Pliensbachian) CO_2 concentrations based on stomatal analysis of fossil conifer leaves from eastern Australia. *Gondwana Research*, *27*(3), 932–939. https://doi.org/10.1016/j.gr.2013.08.021

Steinthorsdottir, M., Vajda, V., & Pole, M. (2016). Global trends of pCO_2 across the Cretaceous-Paleogene boundary supported by the first Southern Hemisphere stomatal proxy-based pCO_2 reconstruction. *Palaeogeography, Palaeoclimatology, Palaeoecology*, *464*, 143–152. https://doi.org/10.1016/j.palaeo.2016.04.033

Steinthorsdottir, M., Vajda, V., & Pole, M. (2019). Significant transient pCO_2 perturbation across the New Zealand Oligocene-Miocene transition recorded by fossil plants. *Palaeogeography, Palaeoclimatology, Palaeoecology*, *515*, 152–161. https://doi.org/10.1016/j.palaeo.2018.01.039

Steinthorsdottir, M., Vajda, V., Pole, M., & Holdgate, G. (2019). Moderate levels of Eocene pCO_2 indicated by fossil plant stomata. *Geology*, *47*(10), 914–918. https://doi.org/10.1130/G46274.1

Steinthorsdottir, M., Wohlfarth, B., Kylander, M. E., Blaauw, M., & Reimer, P. J. (2013). Stomatal proxy record of CO_2 concentrations from the last termination suggests an important role for CO_2 at climate change transitions. *Quaternary Science Reviews*, *68*, 43–58. https://doi.org/10.1016/j.quascirev.2013.02.003

Stoll, D. K., Guitian, J., Hernandez-Almeida, I., Mejia, L. M., Phelps, S., Polissar, P., et al. (2019). Upregulation of phytoplankton carbon concentrating mechanisms during low CO_2 glacial periods and implications for the phytoplankton pCO_2 proxy. *Quaternary Science Reviews*, *208*, 1–20. https://doi.org/10.1016/j.quascirev.2019.01.012

Sun, B.-N., Ding, S.-T., Wu, J.-Y., Dong, C., Xie, S., & Lin, Z.-C. (2012). Carbon isotope and stomatal data of late Pliocene Betulaceae leaves from SW China: Implications for palaeoatmospheric CO_2-levels. *Turkish Journal of Earth Sciences*, *21*, 237–250.

Tesfamichael, T., Jacobs, B., Tabor, N., Michel, L., Currano, E., Feseha, M., et al. (2017). Settling the issue of "decoupling" between atmospheric carbon dioxide and global temperatures: $[CO_2]_{atm}$ reconstructions across the warming Paleogene-Neogene divide. *Geology*, *45*(11), 999–1002. https://doi.org/10.1130/G39048.1

Tipple, B. J., Meyers, S. R., & Pagani, M. (2010). Carbon isotope ratio of Cenozoic CO2: A comparative evaluation of available geochemical proxies. *Paleoceanography*, *25*, PA3202.

van Hoof, T. B., Kürschner, W. M., Wagner, F., & Visscher, H. (2006). Stomatal index response of *Quercus robur* and *Quercus petraea* to the anthropogenic CO_2 increase. *Plant Ecology*, *183*(2), 237–243. https://doi.org/10.1007/s11258-005-9021-3

Wagner, F. (1998). *The influence of environment on the stomatal frequency in Betula*. Ph.D. Thesis, *LPP Contribution series*, *9*, (p. 102). The Netherlands: Utrecht University.

Wagner, F., Below, R., DeKlerk, P., Dilcher, D. L., Joosten, H., Kürschner, W. M., & Visscher, H. (1996). A natural experiment on plant acclimation: Lifetime stomatal frequency response of an individual tree to annual atmospheric CO_2 increase. *Proceedings of the National Academy of Sciences of the United States of America, 93*, 11705–11708.

Wagner, F., Dilcher, D. L., & Visscher, H. (2005). Stomatal frequency responses in hardwood-swamp vegetation from Florida during a 60-year continuous CO_2 increase. *American Journal of Botany*, *92*(4), 690–695. https://doi.org/10.3732/ajb.92.4.690

Wang, H., Leng, Q., Liu, W., & Yang, H. (2017). A rapid lake-shallowing event terminated preservation of the Miocene Clarkia Fossil Konservat-Lagerstätte (Idaho, USA). *Geology*, *45*(3), 239–242. https://doi.org/10.1130/G38434.1

Woodward, F. I. (1987). Stomatal numbers are sensitive to increase in CO_2 from pre-industrial levels. *Nature*, *327*(6123), 617–618. https://doi.org/10.1038/327617a0

Yang, H., Smiley, C. J., Sprenke, K. F., Rember, W. C., & Knowles, C. R. (1995). Subsurface evidence for a rapid formation of the Clarkia Miocene Lake in northern Idaho. *Northwest Science*, *69*, 52–59.

Zachos, J. C., Dickens, G. R., & Zeebe, R. E. (2008). An early Cenozoic perspective on greenhouse warming and carbon-cycle dynamics. *Nature*, *451*(7176), 279–283. https://doi.org/10.1038/nature06588

Zachos, J. C., Pagani, M., Sloan, L., Thomas, E., & Billups, K. (2001). Trends, rhythms and aberrations in global climate 65 ma to present. *Science*, *292*(5517), 686–693. https://doi.org/10.1126/science.1059412

Zhang, Y. G., Pagani, M., Bohaty, S. M., & DeConto, R. (2013). A 40-million-year historyof atmospheric CO_2. *Philosophical Transactions of the Royal Society A*, *371*, 20130096, 2001. https://doi.org/10.1098/rsta.2013.0096

Zhou, N., Wang, Y., Ya, L., Porter, A. S., Kürschner, W. M., Li, L., et al. (2020). An inter-comparison study of three stomatal-proxy methods for CO_2 reconstruction applied to early Jurassic Ginkgoales plants. *Palaeogeography, Palaeoclimatology, Palaeoecology*, *542*, 109547. https://doi.org/10.1016/j.palaeo.2019.109547